Effective PDT/PTT dual-modal phototherapeutic killing of bacteria by using poly(N-phenylglycine) nanoparticles

Sena Ghayyem, Alexandre Barras, Farnoush Faridbod, Sabine Szunerits, Rabah Boukherroub

Microchimica Acta _####################_
https://doi.org/10.1007/s00604-022-05181-0

ORIGINAL PAPER

Effective PDT/PTT dual-modal phototherapeutic killing of bacteria by using poly(N-phenylglycine) nanoparticles

Sena Ghayyem[1,2] · Alexandre Barras[1] · Farnoush Faridbod[2] · Sabine Szunerits[1] · Rabah Boukherroub[1]

Received: 21 September 2021 / Accepted: 7 January 2022

Abstract

This study investigated, for the first time, the antimicrobial properties of polyethylene glycol-functionalized poly(*N*-phenylglycine) nanoparticles (PNPG-PEG NPs). PNPG-PEG NPs exhibit high extinction coefficient in the near-infrared (NIR) region; they can convert light energy into heat energy with high thermal transformation efficiency. Additionally, they can generate cytotoxic reactive oxygen species (ROS) upon light irradiation. Also, PNPG-PEG NPs are not cytotoxic. All these properties make them appropriate for combined dual-modal photothermal and photodynamic therapies. The antibacterial activity of PNPG-PEG NPs was assessed using *Escherichia coli* (Gram-negative) and *Staphylococcus aureus* (Gram-positive) pathogenic strains. The results revealed that NIR light (810 nm) irradiation for 10 min could kill effectively the planktonic bacteria and destroy *Escherichia coli* and *Staphylococcus aureus* biofilms. The results demonstrated that PNPG-PEG NPs represent a very effective nanoplatform for killing of pathogenic bacteria.

Keywords Polymer-based nanomaterials · Antibacterial therapy · Escherichia coli · Staphylococcus aureus · Biofilm

Introduction

Pathogenic bacteria in food and water, even in infinitesimal quantities, seriously affect human health [1]. *Staphylococcus aureus* (*S. aureus*) and *Escherichia coli* (*E. coli*) are among the most rampant species of Gram-positive and Gram-negative bacteria, respectively [2]. *E. coli* is one of the leading causes of nosocomial urinary-tract infections and enterocolitis [3]. *S. aureus* is also an etiological infection agent responsible for considerable diseases and mortality [4]. In the meantime, the usage of conventional antibiotics for treating bacterial infections has become less efficient due to increased rates of antibiotic resistance [5]. Therefore, novel approaches and new antibacterial materials are critical for the effective killing of pathogenic bacteria.

Recently, photodynamic therapy (PDT) and photothermal therapy (PTT) using nanomaterials have received significant attention as therapeutic alternatives due to their high efficiency and reduced toxicity [6]. In PTT, photo-absorbing agents with high thermal transformation efficiency are gathered in the vicinity of the bacteria, and upon light irradiation, they convert light energy into heat energy to cause cell damage and further bacterial eradication [7]. In PTT, although visible light can be used, NIR light is generally preferred, owing to its enhanced depth penetration and reduced damage to biological matter [8, 9]. PTT materials commonly include three types of nanomaterials: (a) inorganic, such as gold [10–12], silver [13], palladium [14], ruthenium [10], and copper-based nanomaterials [15]; (b) organic, such as graphene [16–18] and carbon-based nanomaterials [19]; and (c) polymers, such as polyaniline (PANI)- [20], polypyrrole- [21], polythiophene- [22], polydopamine- [22], and polyvinylpyrrolidone-based nanomaterials [23]. There are a few studies on the use of inorganic nanomaterials as PTT agents for killing bacteria. Although these nanomaterials are good photo-absorbing agents with high thermal transformation efficiency, they are non-biodegradable and generally remain in the body for long periods of time, which grows

Sena Ghayyem and Alexandre Barras contributed equally to this work.

✉ Rabah Boukherroub
rabah.boukherroub@univ-lille.fr

[1] Univ. Lille, CNRS, Centrale Lille, Univ. Polytechnique Hauts-de-France, UMR 8520 - IEMN, F-59000 Lille, France

[2] Analytical Chemistry Department, School of Chemistry, College of Science, University of Tehran, 1417935840 Tehran, Iran

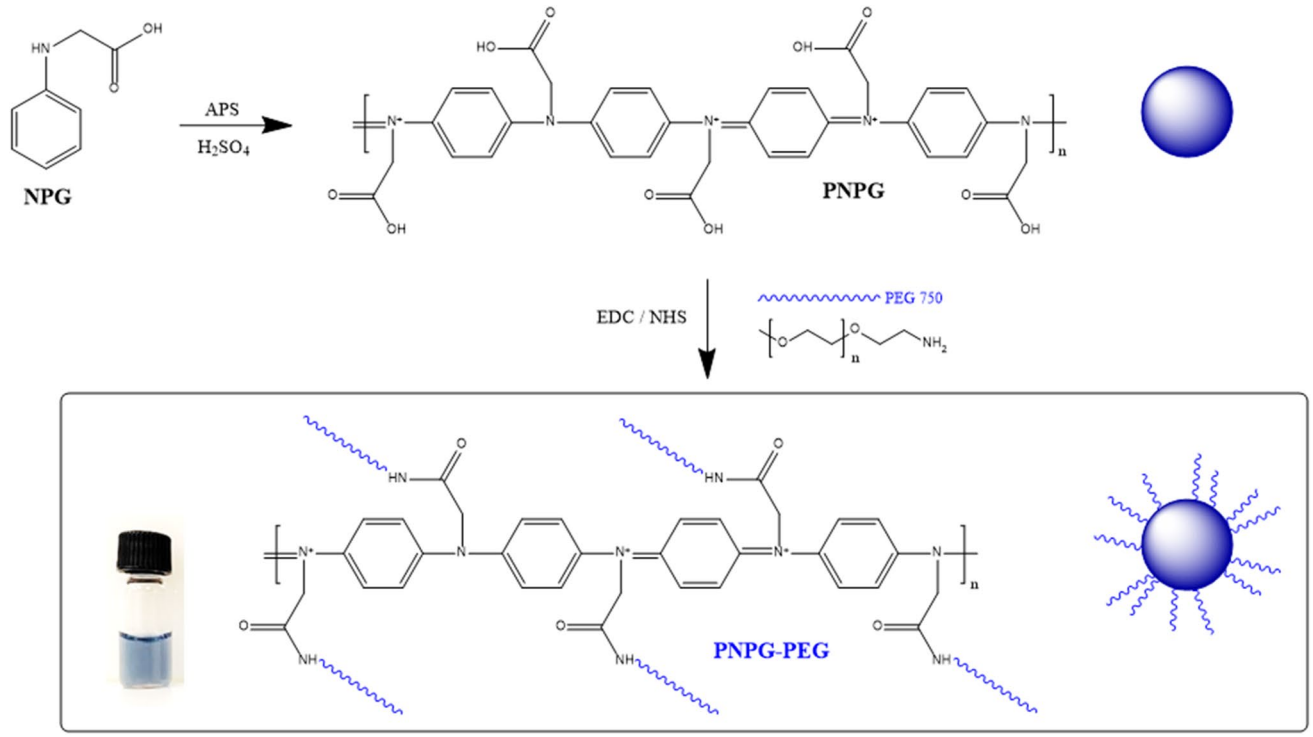

Scheme 1. Schematic illustration of the preparation of polyethylene glycol-functionalized poly(*N*-phenylglycine) nanoparticles (PNPG-PEG NPs) (counterions are omitted for clarity). Inset: a photograph of PNPG-PEG NPs dispersion in water

concerns for their potential long-term toxicity. In contrast, polymer-based PTT agents are biodegradable, which makes them more beneficial for in vivo applications [24]. Overall, polymer-based nanomaterials are considered to be ideal candidates for antibacterial therapy, because of their outstanding properties such as the good ability to absorb NIR radiation, high thermal transformation efficiency, excellent chemical/photo/thermal-stability, low toxicity, and good biocompatibility [25].

PDT requires the use of a photosensitizer (PS) able to generate reactive oxygen species (ROS), upon light irradiation at an appropriate wavelength in presence of molecular oxygen, to kill pathogenic bacteria. In PDT, the PS transfers energy to the surrounding oxygen to generate cytotoxic ROS, resulting in DNA/protein/lipid damage and finally cell death [25]. PDT photosensitizers can be divided into porphyrins, chlorine, and dyes [26]. These PSs are typically activated by applying UV–visible light, which is not suitable for clinical implementation [27]. Recently, a few studies have focused on the design and construction of new PSs that can generate ROS and damage cellular components in the presence of an external NIR light source [28, 29].

Multimodal therapy by delivering different types of treatments together has become a hopeful approach to improve therapeutic efficacy. Compared with PDT or PTT alone, integrating PDT with PTT can enhance antibacterial eradication [28]. A few studies about the use of inorganic nanomaterials for dual-mode phototherapeutic treatment of bacterial infections have been reported [27, 28, 30], but reports about the use of polymer-based nanomaterials for PTT or PDT treatment of bacterial infections are scarce. One of the reports on the antibacterial properties of polymer-based nanomaterials is that by Xing et al., consisting of an anionic water-soluble polythiophene (PTP) and a cationic porphyrin (TPPN), which can form a complex that can generate singlet oxygen after irradiation [30]. Hsiao et al. described a chitosan (CS) derivative with self-doped polyaniline (PANI) side chains that can convert NIR light into heat to kill bacteria [6].

Poly(*N*-phenylglycine) (PNPG) is an analogue of polyaniline (PANI) obtained by *N*-phenylglycine (NPG) chemical polymerization. While PNPG is not water dispersible, its dispersion in aqueous media can be improved through chemical functionalization with polyethylene glycol amine (PEG) [24]. In this work, we synthesized water dispersible PNPG-PEG nanoparticles (Scheme 1) according to our previous report [31] and investigated, for the first time, their antibacterial properties under NIR light irradiation. We demonstrated that PNPG-PEG nanoparticles can be used as a novel PTT/PDT agent under 810 nm irradiation to stimulate the production of a great amount of heat and ROS to kill bacteria.

Experimental section

NIR light-mediated antibacterial activity of PNPG-PEG NPs

The antibacterial activity of PNPG-PEG NPs was assessed using *Escherichia coli* K-12 MG1655 (Gram-negative) and *Staphylococcus aureus* 43300 MRSA (Gram-positive) pathogenic strains. Glycerol stocks (− 80 °C) of *E. coli* and *S. aureus* were streaked out on LB (Luria–Bertani) and BHI (Brain Heart Infusion) agar plates, respectively. *E. coli* and *S. aureus* cultures were grown on nutrient agar for 24 h.

A single *E. coli* and *S. aureus* colony from LB/BHI agar plate was inoculated for 6 h in LB/BHI medium at 35 °C, 200 rpm in an orbital shaker incubator (Labnet 211DS). Afterwards, the medium was separated by centrifugation, the pellet re-suspended in PBS, and the final bacterial concentration was adjusted to 10^6 or 10^{10} CFU mL^{-1}. To assess the antibacterial properties of PNPG-PEG NPs, 600 µL of the bacterial solution was added to different concentrations (10, 25, 50, and 100 µg mL^{-1}) of PNPG-PEG NPs in PBS at a final volume of 1 mL and the reaction mixture was incubated at 35 °C for 30 min. After incubation, wells were irradiated for 10 min at 1.5 W cm^{-2}. Both irradiated and non-irradiated (controls) solutions were diluted, and an appropriate amount was placed on agar plates and incubated at 37 °C. After 24 h, both irradiated and non-irradiated (controls) colonies were counted.

Intracellular relative reactive oxygen species (ROS) production

In order to examine the production of intracellular ROS, DCFH-DA was used [31]. One colony from the plates was transferred into 3 mL TSB and incubated at 35 °C, 200 rpm in an orbital shaker incubator (Labnet 211DS) until it reached the exponential growth phase (OD_{600} = 0.5–1.0; GeneQuant *pro*, Amersham Biosciences). The cell suspensions were stained with 10 µM DCFH-DA for 30 min and then washed once by centrifugation (3500 g for 5 min; Eppendorf 5804) with PBS (pH 7.4; Gibco®). The pellets were resuspended in PBS, and the final bacterial concentration was adjusted to 10^7 CFU mL^{-1}. After that, the bacteria samples were treated with PNPG-PEG NPs (100 µg mL^{-1}) in PBS for 30 min and then irradiated with a continuous laser (810 nm, 1.5 W cm^{-2}). Treated cells, cells alone with or without irradiation stained with DCFH-DA, served as the negative controls. Relative fluorescence intensities were recorded in a 24-well cell culture plate from the bottom using a Cytation™ 5 Cell Imaging Multi-Mode Reader (BioTek Instruments SAS, France) at an excitation/emission wavelength of 485–20/528–57 nm.

NIR light-mediated biofilm destruction of PNPG-PEG NPs

One colony from the plates was transferred into 3 mL TSB and incubated overnight at 35 °C, 200 rpm in an orbital shaker incubator (Labnet 211DS). After 18 h, the inocula were prepared by diluting the overnight cultures 1:100 in TSB (0.5X) supplemented with additional glucose to a final concentration of 1%. One mL of the inoculum was transferred to the assay wells of a sterile 24-well assay plate (Thermo Scientific™, Nunc™ MicroWell™, Nunclon Delta-Treated, Flat-Bottom Microplate), which corresponds to an inoculum of approximately $0.5–1 \times 10^7$ cells/well. Each plate was covered with an adhesive foil lid (Greiner Bio-One GmbH, ViewSeal 676,070). Inoculated plates were transferred to an incubator set at 35 °C and incubated for 48 h without shaking. After incubation, biofilms were washed with 0.9% saline solution in order to remove planktonic bacteria.

The biofilms grown on plastic assay wells were incubated with a solution of PNPG-PEG NPs (100 µg mL^{-1} in PBS) and then irradiated with a laser (810 nm, 1.5 W cm^{-2}) for 10 min. Following this treatment, cells were detached from the bottom and homogenized in liquid medium via scraping and vortexing. In order to estimate the viability of cells detached in the aqueous solution from the biofilm, the plating method was realized by the aseptic removal of aliquots of the suspended biofilm, followed by serial dilution and plating onto TSA nutrient plates. After 24 h incubation, colonies were counted on the plates, and the number of cells per milliliter (CFU mL^{-1}) in the original culture was calculated using the mean colony counts, the volume of culture plated, and the dilution factor from the suspended biofilm to the plate.

The biofilms were also stained with LIVE/DEAD™ Bac Light™ Bacterial Viability Kit (Thermo Fisher Scientific), and both irradiated and non-irradiated (control) biofilms were imaged by fluorescence microscopy using a Cytation™ 5 Cell Imaging Multi-Mode Reader (BioTek Instruments SAS, France) with 20 × objective magnification and with the corresponding excitation and emission filters (469–35/525–39 nm for SYTO™ 9 and 586–15/647–57 nm for propidium iodide).

Statistical analysis

All experiments were conducted with at least duplicate or triplicate observations per condition. Data were analyzed by ordinary one-way or two-way analysis of variance (ANOVA) with Dunnett's multiple comparison test for ROS generation

and cell viability and Holm-Sidak's multiple comparison test for antibacterial activities, and expressed as mean ± SD. *p value < 0.05, **p value < 0.01, ***p value < 0.001, and ****p value < 0.0001 were considered significant compared to a control. Statistical analysis was performed with GraphPad Prism 7 (version 7.05).

Results and discussion

Characterization of polyethylene glycol-functionalized poly(N-phenylglycine) (PNPG-PEG) nanoparticles

The PNPG-PEG NPs investigated in this study were synthesized following the process in Scheme 1. First, PNPG NPs were prepared by oxidative polymerization of *N*-phenylglycine monomer in acidic conditions (0.1 M H_2SO_4) using APS as the oxidant [31]. The acid groups of PNPG NPs were activated using EDC·HCl/NHS, and then amino-PEG (750 Da) was introduced to produce highly dispersible PNPG-PEG NPs (Scheme 1, inset). The successful synthesis of the PNPG-PEG NPs was confirmed by various characterization techniques. The main characterizations of PNPG and PNPG-PEG NPs are reported in our previous work [31].

The morphology of PNPG-PEG NPs was determined by scanning electron microscopy (SEM). The nanoparticle size distribution histogram was realized based on 100 counted nanoparticles. As shown in Fig. 1A, the mean diameter of the PNPG-PEG NPs is 77.3 nm with 22.9 nm standard deviation. The PNPG-PEG NPs have a nearly spherical shape with an average diameter ranging between 35 and 155 nm (Fig. 1A, inset). The mean hydrodynamic average diameter (number) of PNPG-PEG NPs was determined to be 151.5 ± 62.5 nm in water (Fig. 1B) and a surface charge of + 17.5 mV (data not shown), due to the presence of positively charged nitrogen groups.

In PBS buffer, the diameter increased to 339.1 ± 113 nm, immediately after dispersion. Time-dependent stability of the NP dispersions was assessed by DLS in water and PBS (Figure S1A). During 1 h at room temperature, the dispersion remains stable in water, while the hydrodynamic diameter increases in PBS due to aggregates' formation. The dispersibility of the synthesized PNPG-PEG NPs was further examined by their dispersion in different solvents: water, phosphate buffered saline (PBS), Dulbecco's Modified Eagle's Medium (DMEM) with 10% fetal bovine serum, and tryptic soy broth (TSB, bacterial nutrient medium). The NPs are highly dispersible in all solutions (Figure S1B) for several hours at room temperature without any apparent aggregation, due to the excellent colloidal stability provided by the PEG moieties. It is also worth noting that optical observation revealed that after one day, only a very slight sedimentation of NPs was apparent. The phenomenon was higher in PBS due to high salt concentration and phosphate ions. However, all suspensions stayed dispersible with further agitation (Figure S2). The optical properties of PNPG-PEG NPs were examined by using UV–vis-NIR spectroscopy. The UV–vis-NIR absorption spectrum of PNPG-PEG NPs displayed high absorption in the visible region (500–780 nm) and NIR region up to 900 nm (Figure S1C). The most attractive feature was still the high optical absorption of PNPG-PEG NPs at 810 nm (Figure S1D), which increases with the nanoparticle concentration and makes them an effective photothermal agent for antimicrobial therapy by means of local hyperthermia.

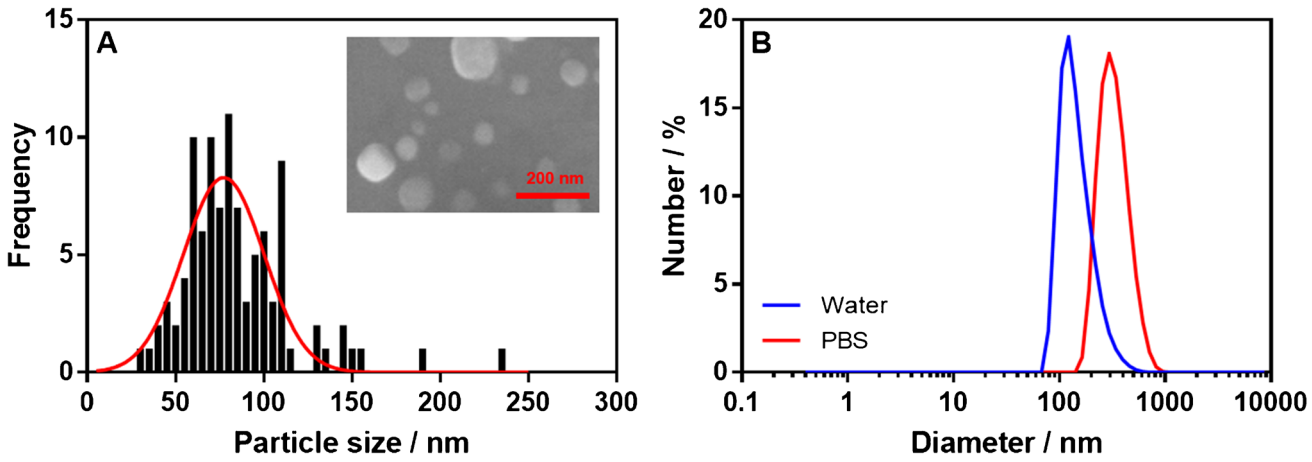

Fig. 1 **A** Particle size distribution histogram of PNPG-PEG NPs and SEM image (inset) of PNPG-PEG NPs. **B** Analysis of nanoparticle size (diameter in number) by DLS in water (blue) and PBS (10 µg mL^{-1}, red)

Photothermal and photodynamic properties of PNPG-PEG nanoparticles

The photothermal properties of different concentrations of PNP-PEG NPs were first assessed upon irradiation with a continuous laser (810 nm, 0.7 W cm^{-2}) for 10 min (Fig. 2A). The temperature of the dispersions increases in a concentration- and a time-dependent manner to reach rapidly 52 °C in 10 min for a concentration of 100 µg mL^{-1} in water.

The photothermal properties of different concentrations of PNP-PEG NPs were further studied at different power densities (1.0 and 1.5 W cm^{-2}) upon 10-min laser irradiation (Figure S3). The temperature profiles of PNPG-PEG NPs are depicted in Fig. 2B, indicating that the photothermal heating effect could increase monotonically with the concentration of NPs and power density. For all investigated concentrations of NPs at a power density of 1.5 W cm^{-2}, the temperature reaches 65 °C after 10-min laser irradiation. These observations indicate that these nanoparticles have the potential to convert light energy into heat energy. These good photothermal properties demonstrate that PNPG-PEG NPs can be applied as a PTT agent for killing bacteria.

Conjugated polymer NPs are able to generate reactive oxygen species (ROS) upon laser irradiation and act as photodynamic therapy (PDT) agents [32]. The ROS generation by PNPG-PEG NPs was indirectly examined using 2′,7′-dichlorofluorescin (DCFH) probe. DCFH can be easily oxidized to the highly fluorescent product (DCF, dichlorofluorescein) by oxygen radical anion ($O_2^{\bullet-}$) and singlet oxygen ($^1O_2$). Therefore, ROS generation can be investigated by following the increase in the fluorescence emission intensity of DCFH. For this purpose, PNPG-PEG NPs were mixed with deacetylated DCFH-DA solution and irradiated with 810 nm laser at 1.5 W cm^{-2} (Figure S4). Changes in the fluorescence emission were immediately recorded after irradiation. As a control, the changes in the fluorescence emission of DCFH alone without nanoparticles were investigated. After 10-min laser irradiation, almost no fluorescence was observed. The fluorescence emission at 528 nm increased by increasing the PNPG-PEG NPs concentration, suggesting ROS generation under laser (NIR); a similar behavior was observed upon laser irradiation while keeping the plate on ice (NIR at 4 °C) in order to compensate the PTT effect. The thermal temperature elevation with 100 µg mL^{-1} of PNPG-PEG solutions on ice (similar setup for all experiments) were measured and presented in Figure S3C. Furthermore, the fluorescence intensity recorded at room temperature and at 4 °C was much lower than that measured under laser irradiation on ice. The fluorescence increase was non-negligible at 65 °C (direct heating) even though it is less significant compared to that recorded under laser irradiation for all concentrations. This evidence confirms the ROS generation capability of PNPG-PEG NPs.

Cytotoxicity assay

In order to evaluate cell viability, metabolic activity was assessed using a standard resazurin assay. For this purpose, HeLa and U-87 MG cells were exposed to PNPG-PEG NPs at concentrations ranging from 0 to 100 µg mL^{-1} in DMEM containing fetal bovine serum (FBS) for 24 h. As shown in Fig. 3A, all cell viabilities for HeLa and U-87 MG were, respectively, higher than 90% and 80% at the highest PNPG-PEG concentration of 100 µg mL^{-1}. These results revealed that PNPG-PEG NPs present minor dark cytotoxicity in vitro in the concentration range up to 100 µg mL^{-1}.

Encouraged by efficient phototoxicity (PTT and PDT effects) of the PNPG-PEG NPs in solution mentioned above,

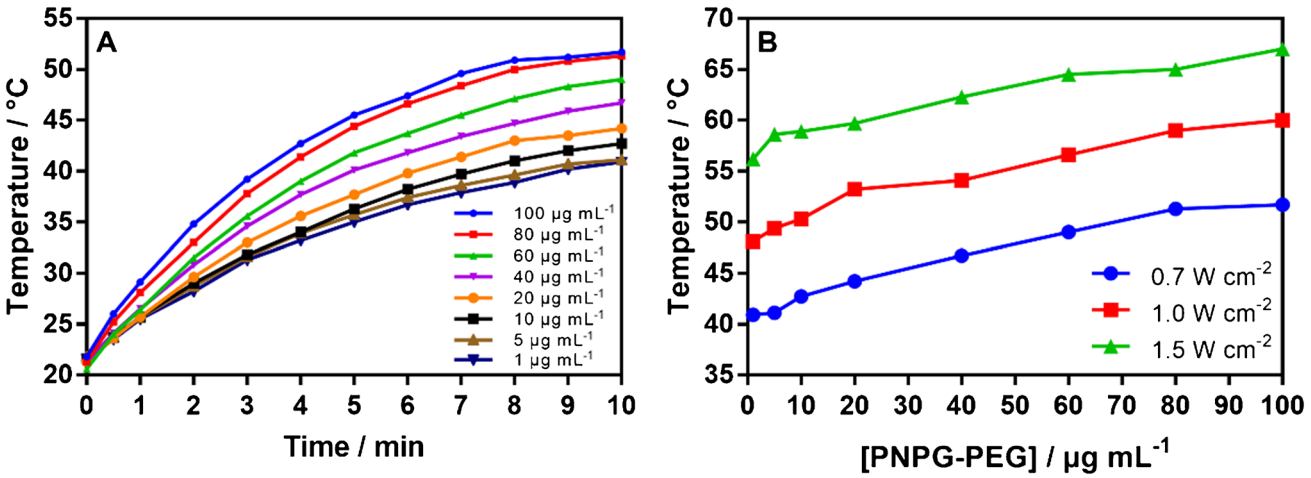

Fig. 2 **A** Temperature evolution as a function of PNPG-PEG NPs concentration in water upon 10-min laser irradiation (810 nm, 0.7 W cm^{-2}). **B** Temperature profiles of PNPG-PEG NPs after 10 min irradiation (810 nm) at different laser power densities (0.7, 1, and 1.5 W cm^{-2})

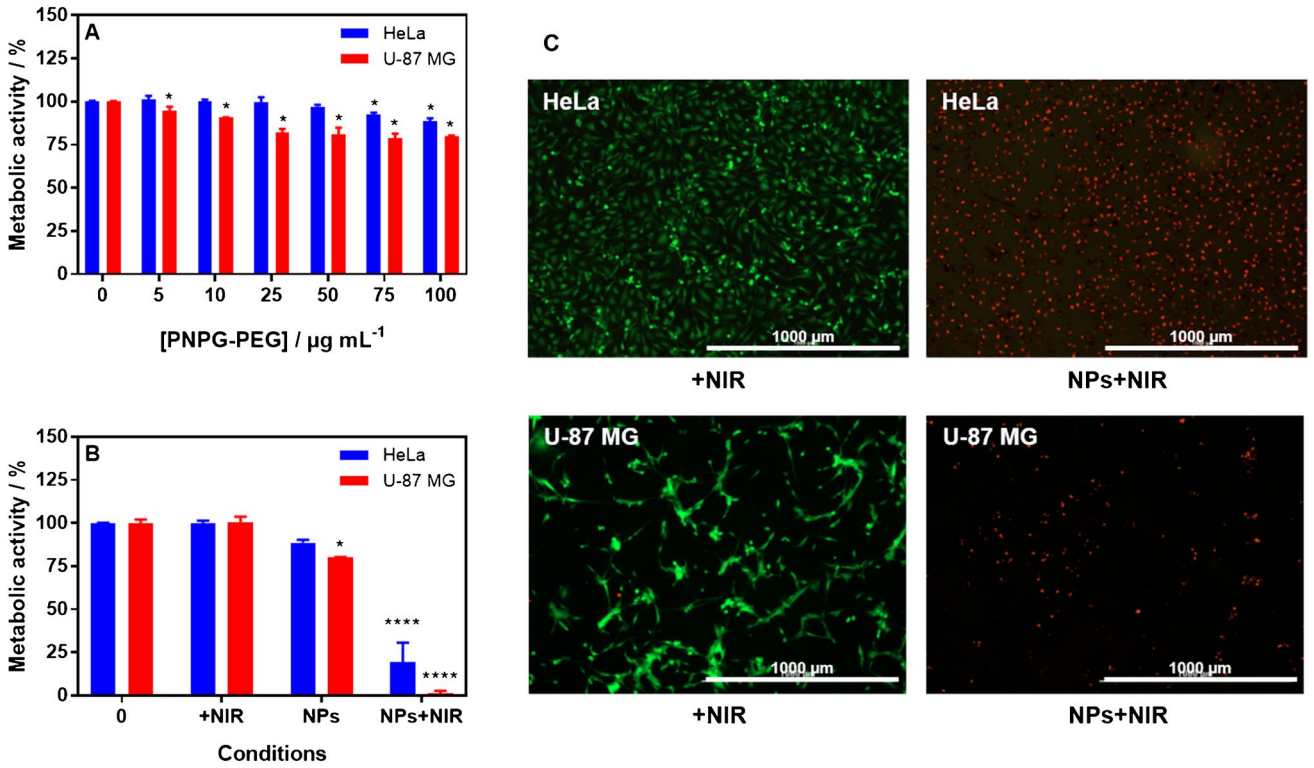

Fig. 3 **A** Relative viability of HeLa and U-87 MG cells incubated with different concentrations of PNPG-PEG NPs for 24 h (*$p < 0.05$, significance versus control, $n = 3$). **B** Relative photoinduced viability of HeLa and U-87 MG cells incubated with 100 μg mL^{-1} of PNPG-PEG NPs for 24 h and irradiated with the 810 nm laser at 1.5 W cm^{-2} (*$p < 0.05$, and ****$p < 0.0001$, significance versus control, $n = 2$). **C** Fluorescence microscopy images of HeLa and U-87 MG cells treated or not with PNPG-PEG NPs (100 μg mL^{-1}) for 24 h, irradiated at 810 nm for 10 min (1.5 W cm^{-2}) and stained with calcein-AM (green, living cells) and propidium iodide (PI, red, dead cells)

the photocytotoxicity effect on both cells was further studied under 810-nm laser irradiation during 10 min after 24 h incubation with PNPG-PEG NPs at 100 μg mL^{-1}. After incubation, cells were irradiated for 10 min at 1.5 W cm^{-2} and incubated for further 24 h before the assay. As shown in Fig. 3B, the cell viability of the control (cells alone under laser irradiation) remained at 100% following laser irradiation for both HeLa and U-87 MG cells. These results revealed that the irradiation alone did not affect the cell viability. On the contrary, viability of the cells previously incubated with 100 μg mL^{-1} of PNPG-PEG NPs significantly decreased by 80% and 98.5% for HeLa and U-87 MG, respectively, upon 10-min laser illumination at 1.5 W cm^{-2}, confirming the apparent PDT and PTT effects of the nanoparticles.

Moreover, dead and live cells were imaged by staining the cells with calcein-AM and PI in order to confirm the metabolic activity results. As shown in Fig. 3C, control cells irradiated with 810 nm laser at a power density of 1.5 W cm^{-2} for 10 min displayed green emission (live cells), confirming that the 810 nm laser had no effect on the cell viability. In the opposite, when cells were previously treated with NPs (100 μg mL^{-1}) and 810-nm laser illumination, most of cells exhibited red emission (dead cells), indicating that both cell lines were killed due to combined phototoxicity effects.

Photothermal/photodynamic killing of bacteria

Considering the efficient photothermal and photodynamic effects of PNPG-PEG NPs in aqueous solution and in vitro on eukaryotic cells, we chose to study their potential as PTT and PDT agent for killing bacteria in vitro. The antibacterial activity of PNPG-PEG NPs was assessed using both Gram-positive *S. aureus* and Gram-negative *E. coli* bacteria as the bacterium models at the final concentrations of 5×10^5 and 5×10^9 CFU mL^{-1}. For this purpose, to a bacterial solution was added different concentrations (10, 25, 50, and 100 μg mL^{-1}) of PNPG-PEG NPs in PBS, and the reaction mixture was incubated at 37 °C for 30 min. After incubation, wells were irradiated for 10 min at 1.5 W cm^{-2}. Then, both irradiated and non-irradiated (controls) solutions were diluted and an appropriate amount was placed on agar plates and incubated at 37 °C. After 24 h, both irradiated and non-irradiated (controls) colonies were counted. As shown in Fig. 4, the bacterial viability decreased with increasing the concentration of PNPG-PEG

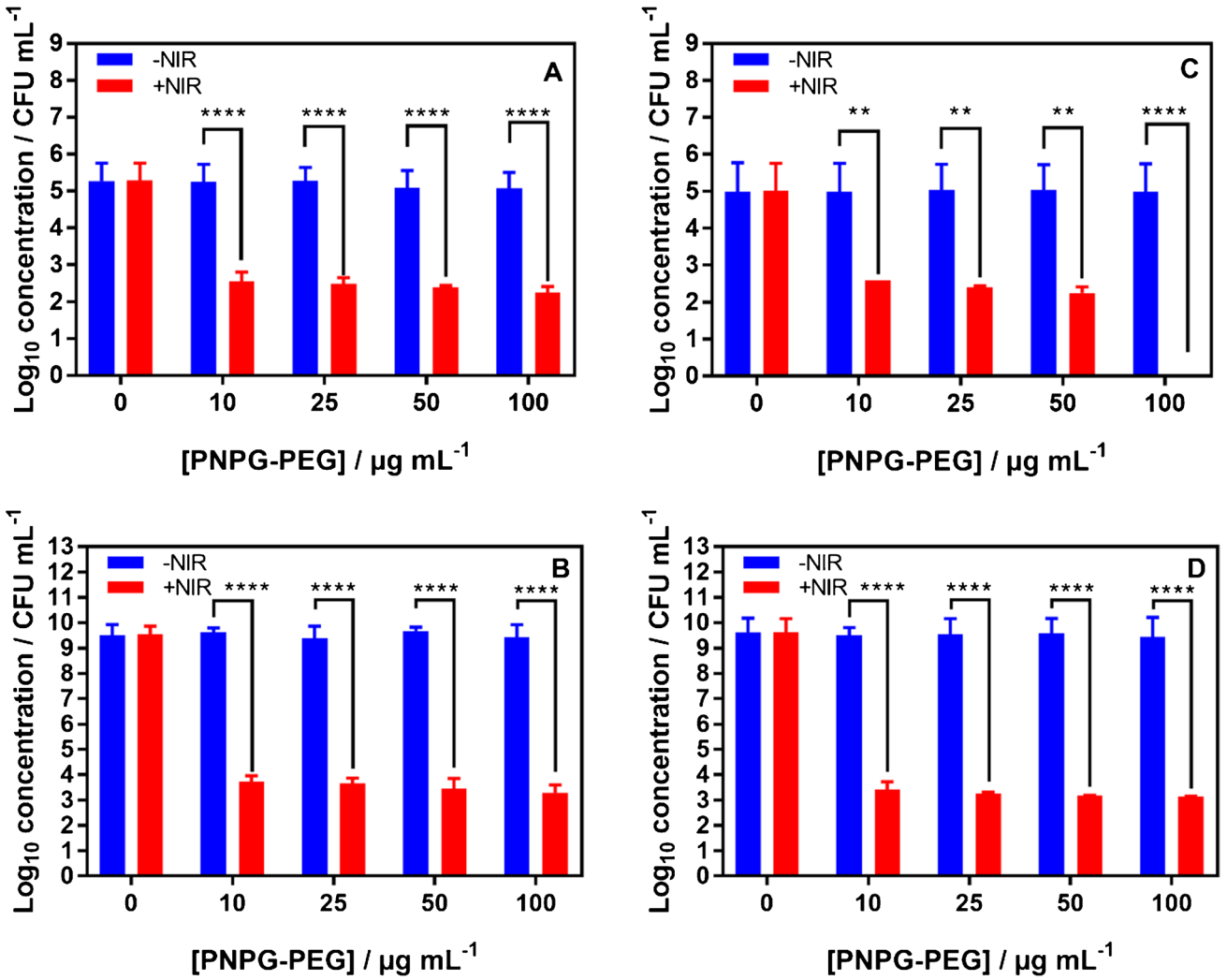

Fig. 4 Logarithmic bacterial viability of different concentrations of PNPG-PEG NPs under PTT/PDT treatment for *E. coli* at a final bacterial concentration of **A** 5×10^5 CFU mL^{-1} and **B** 5×10^9 CFU mL^{-1}, *S. aureus* at a final bacterial concentration of **C** 5×10^5 CFU mL^{-1} and **D** 5×10^9 CFU mL^{-1} under 810-nm laser irradiation at 1.5 W cm^{-2} for 10 min (**$p<0.01$ and ****$p<0.0001$, +NIR versus -NIR, $n=2$)

NPs. Using 100 μg mL^{-1} of PNPG-PEG NPs suspension, only 1.3×10^2 and 3.3×10^3 CFU mL^{-1} of *E. coli* bacteria survived after irradiation of 5×10^5 and 5×10^9 CFU mL^{-1} for 10 min, respectively. This result contrasts somehow with that recorded for *S. aureus* bacteria with full eradication after 10 min irradiation at 810 nm at a bacterial concentration of 5×10^5 CFU mL^{-1}. Using a bacterial concentration of 5×10^9 CFU mL^{-1}, 1.3×10^3 CFU mL^{-1} of bacteria survived under otherwise similar treatment.

Reports about the use of polymer-based nanomaterials for PTT or PDT treatment of bacterial infections are scarce. Table 1 compares the efficiency of the PNPG-PEG NPs with other PDT/PTT polymer-based nanomaterials reported in the literature. It can be seen that the PNPG-PEG NPs have a great potential for killing of planktonic cells compared to other polymer-based nanomaterials.

In order to estimate the PDT effect in vitro on bacteria survival, the experiments were also carried out at 4 °C. For this purpose, both *S. aureus* and *E. coli* bacteria (5×10^5 CFU mL^{-1}) were examined. As shown in Figure S5, the effect of PDT alone on bacteria killing is less pronounced than that of PTT alone. Using 100 μg mL^{-1} of PNPG-PEG NPs suspension, the decreasing trend of cell viability corresponds to less than 1 log for *E. coli* and *S. aureus* after irradiation on ice (4 °C) of 5×10^5 for 10 min. At high concentrations, the temperature increase is significant (Figure S3C) to rule out a photothermal effect on cell

Table 1 Comparison of the PNPG-PEG NPs with other PDT/PTT polymer-based nanomaterials

Polymer-based nanomaterials	Bacteria treated	Reduction of bacterial viability	Reference
Anionic polythiophene (PTP) & a cationic porphyrin (TPPN) (PTP/TPPN complex)	*E. coli* *B. subtilis*	70% 90%	[30]
Self-doped *N*-(mercaptopropylsulfonic acid substituted PANI)-CS (NMPA-CS)	MRSA	94%	[6]
Cationic poly(arylene ethynylene) conjugated polyelectrolytes	*P. aeruginosa*	80%	[33]
PDPP-DBT nanoparticles modified with the Tat peptide (RKKRRQRRRC) (CPNs-Tat)	*S. aureus* *C. albicans* *E. coli*	90% 100% 99.8%	[34]
PNPG-PEG	*E. coli* *S. aureus*	99.97% 100%	**This work**

viability. Although we have demonstrated oxygen generation of nanoparticles in vitro (Fig. 2C), it seems that the share of reactive species is not sufficient to visualize a PDT effect alone in the presence of bacteria in solution.

To further investigate the PDT effect, we measured the intracellular ROS production by bacteria. For this purpose, bacterial inocula were first incubated with DCFH-DA solution for 30 min. Then, bacterial solutions were incubated with PNPG-PEG NPs alone or irradiated with 810 nm laser at 1.5 W cm^{-2}. Changes in the fluorescence emission were recorded after irradiation. As shown in Fig. 5A, a significant increase of fluorescence emission at 528 nm was observed only with PNPG-PEG NPs under laser illumination for *E. coli* and *S. aureus*, suggesting ROS generation. As a control (Fig. 5B), the changes in the fluorescence emission of DCF were investigated by incubation of PNPG-PEG NPs with bacteria at 65 °C. Fluorescence analysis further indicated a 1.4-fold increase in ROS level upon incubation of PNPG-PEG NPs with *E. coli* at 65 °C, in comparison with untreated control at room temperature, indicating lower oxidant activity than laser treated samples (3.7-fold increase). For *S. aureus*, the fluorescence intensity featured a 3.8-fold increase in ROS level, which is much lower than the laser treated sample (6.5-fold increase). This evidence only confirms the partial ROS production of PNPG-PEG NPs in vitro.

The evaluation of bacterial killing in solution after 10 min in an incubator set at 65 °C are presented in Figure S6 in order to evaluate the contribution of heat. Using a bacterial concentration of 5×10^9 CFU mL^{-1}, bacteria survived without any significant loss of viable cells. *E. coli* in solution at 5×10^5 CFU mL^{-1} also survived under these conditions. For *S. aureus*, a slight decrease (0.2 log) in cell viability was detected. Taken together, these nanoparticles exhibit a local photothermal effect on both Gram-positive and Gram-negative bacteria.

Bacteria biofilm destruction

The bacteria within a biofilm are 10–1000 times more resistant than planktonic cells, and it is difficult to destroy bacterial biofilms [34]. There are many reports about the treatment of planktonic bacteria, but reports about the treatment of biofilms are scarce [33]. In this study, we assessed the capability of PNPG-PEG NPs to eradicate *E. coli* and *S. aureus* biofilms upon irradiation with an 810 nm laser for 10 min at 1.5 W cm^{-2} by using the counting method. The viability loss was evaluated by colony counting method on

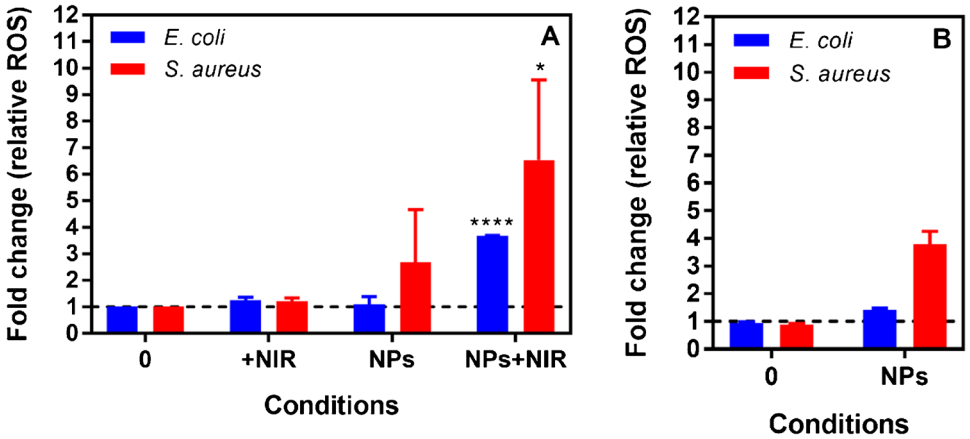

Fig. 5 **A** Intracellular ROS production: relative emission fluorescence intensity (528/20 nm) of bacterial solution incubated with 100 µg mL^{-1} of PNPG-PEG NPs under laser (810 nm) at 1.5 W cm^{-2} for 10 min (*$p > 0.05$ and ****$p < 0.0001$, significance versus control, $n = 2$). **B** Controls at 65 °C (significance versus control at RT, $n = 2$)

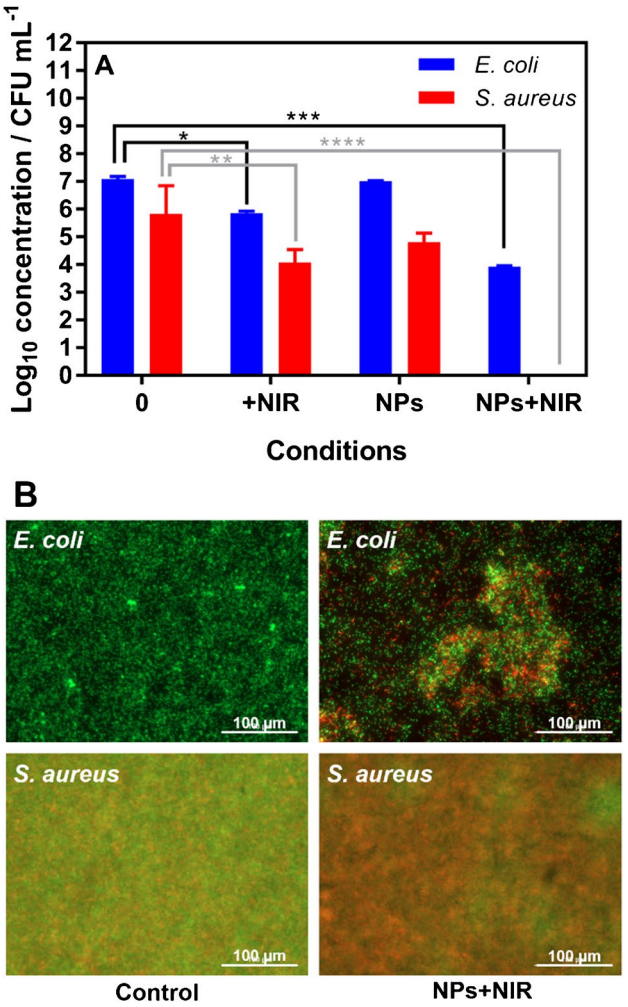

Fig. 6 **A** Logarithmic *E. coli* and *S. aureus* biofilm reduction using PNPG-PEG NPs (100 µg mL^{-1}) under PTT/PDT treatment using 810-nm laser irradiation at 1.5 W cm^{-2} for 10 min $*p<0.05$, $**p<0.01$, $***p<0.001$ and $****p<0.0001$, significance versus control, $n=2$). **B** Fluorescence images of bacterial biofilm stained with calcein-AM (green) and PI (red) after being treated with PNPG-PEG NPs (100 µg mL^{-1}) under NIR laser irradiation (810 nm, 1.5 W cm^{-2}) for 10 min

agar plates. The biofilm cell viability curve is displayed in Fig. 6A. As can be seen, this treatment led to a total decrease in biofilm cell survival for *S. aureus*, while the treatment achieved ~ 3 log decrease in biofilm cell survival for *E. coli*.

The results above were also confirmed by the calcein-AM/propidium iodide (PI) dual fluorescence staining of bacteria using fluorescence microscopy. As depicted in Fig. 6B, untreated *E. coli* and *S. aureus* biofilms emitted green fluorescence, which is indicative of live bacteria in the biofilm. On the contrary, after being treated with PNPG-PEG NPs under NIR laser irradiation (810 nm, 1.5 W cm^{-2}), the observed red fluorescence emission points out the elimination of the bacteria as a result of combined photothermal and photodynamic processes. The decrease of biofilm mass was also observed for *E. coli*.

The SEM images before and after irradiation are displayed in Figure S7. The control *E. coli* biofilm maintained an entire and undamaged rod-shape structure. However, upon incubation with PNPG-PEG NPs + NIR treatment, the biofilm exhibited an evident decline in the biofilm mass. Also, this treatment damaged the bacterial cell membrane and altered the morphology of the biofilm.

Conclusion

We synthesized water dispersible polyethylene glycol-functionalized poly(*N*-phenylglycine) nanoparticles and investigated their photothermal and photodynamic properties. We characterized their function as a dual mode photothermal therapy and photodynamic therapy. Combining with the 810 nm NIR irradiation, the nanoparticles were able to convert light energy into heat energy and generate reactive oxygen species. While the contribution of ROS generation is negligible in the killing mechanism, local heat generation appears to predominate in the death of Gram-negative and Gram-positive bacteria in vitro. Also, in this study, we investigated the capability of these nanoparticles to eradicate *E. coli* and *S. aureus* biofilms upon 810-nm laser irradiation for 10 min. The results revealed that this treatment can decrease the biofilm mass and alter the viability of the biofilm.

Supplementary information.

Supplementary Information The online version contains supplementary material available at https://doi.org/10.1007/s00604-022-05181-0.

Funding This study is financially supported by the Centre National de la Recherche Scientifique (CNRS), the University of Lille, the Hauts-de-France region, and the CPER "Photonics 4 Society" for financial support. This work was partly supported by the French Renatech network.

Declarations

Conflict of interest The authors declare no competing interests.

References

1. J. P. S. Cabral, Water microbiology. bacterial pathogens and water, Int. J. Env. Res. Public Health 7(10) (2010) 3657–3703.
2. Bannerman DD, Paape MJ, Lee JW, Zhao X, Hope JC, Rainard P (2004) *Escherichia coli* and *Staphylococcus aureus* elicit differential innate immune responses following intramammary infection. Clin Vaccine Immunol 11(3):463–472
3. N. Allocati, M. Masulli, M. F. Alexeyev, C. Di Ilio, *Escherichia coli* in Europe: an overview, Clin. Environ. Toxicol. 10(12) (2013) 6235–6254.

4. S. Y. C. Tong, J. S. Davis, E. Eichenberger, T. L. Holland, V. G. Jr. Fowler, *Staphylococcus aureus* infections: epidemiology, pathophysiology, clinical manifestations, and management, Clin. Microbiol. Rev. 28(3) (2015) 603–661
5. Hauser AR, Mecsas J, Moir DT (2016) Beyond antibiotics: new therapeutic approaches for bacterial infections. Clin Infect Dis 63(1):89–95
6. Hsiao CW, Chen HL, Liao ZX, Sureshbabu R, Hsiao HC, Lin SJ, Chang Y, Sung HW (2015) Effective photothermal killing of pathogenic bacteria by using spatially tunable colloidal gels with nano-localized heating sources. Adv Funct Mater 25:721–728
7. Wang S, Riedinger A, Li H, Fu C, Liu H, Li L, Liu T, Tan L, Barthel MJ, Pugliese G, De Donato F, D'Abbusco MS, Meng X, Manna L, Meng H, Pellegrino T (2015) Plasmonic copper sulfide nanocrystals exhibiting near-infrared photothermal and photodynamic therapeutic effects. ACS Nano 9:1788–1800
8. Zhu H, Cheng P, Chen P, Pu K (2018) Recent progress in the development of nearinfrared organic photothermal and photodynamic nanotherapeutics. Biomater Sci 6:746–765
9. H. Zhang, Y. Liang, H. Zhao, R. Qi, Z. Chen, H. Yuan, H. Liang, L. Wang, Dual-mode antibacterial conjugated polymer nanoparticles for photothermal and photodynamic therapy, Macromol. Biosci. 20 (2020) 1900301 (1–7).
10. Hu DF, Li H, Wang BL, Ye Z, Lei WX, Jia F, Jin Q, Ren KF, Ji J (2017) Surface-adaptive gold nanoparticles with effective adherence and enhanced photothermal ablation of methicillin-resistant *Staphylococcus aureus* Biofilm. ACS Nano 11:9330–9339
11. K. Turcheniuk, V. Turcheniuk, C. H. Hage, T. Dumych, R. Bilyy, J. Bouckaert, L. Héliot, V. Zaitsev, R. Boukherroub, S. Szunerits, Highly-effective photodynamic inactivation of *E. coli* using gold nanorods/SiO_2 core–shell nanostructures with embedded verteporfin, Chem. Commun. 51 (2015) 16365–16368.
12. Jijie R, Dumych T, Chengnan L, Bouckaert J, Turcheniuk K, Hage CH, Heliot L, Cudennec B, Dumitrascu N, Boukherroub R, Szunerits S (2016) Particle-based photodynamic therapy based on indocyanine green modified plasmonic nanostructures for inactivation of a Crohn's disease-associated *Escherichia coli* strain. J Mater Chem B 4:2598–2605
13. D'Agostino A, Taglietti A, Desando R, Bini, M, Patrini M, Dacarro G, Cucca L, Pallavicini P, Grisoli P (2017) Bulk surfaces coated with triangular silver nanoplates: Antibacterial action based on silver release and photo-thermal effect. Nanomaterials 7:7
14. Xiao JW, Fan SX, Wang F, Sun LD, Zheng XY, Yan CH (2014) Porous Pd nanoparticles with high photothermal conversion efficiency for efficient ablation of cancer cells. Nanoscale 6:4345–4351
15. Tao B, Lin C, Deng Y, Yuan Z, Shen X, Chen M, He Y, Peng Z, Hu Y, Cai K (2019) Copper nanoparticles-embedded hydrogel for killing bacteria and promoting wound healing with photothermal therapy. J Mater Chem B 7:2534–2548
16. Jia X, Ahmad I, Yang R, Wang C (2017) Versatile graphene-based photothermal nanocomposites for effectively capturing and killing bacteria, and for destroying bacterial biofilms. J Mater Chem B 5:2459–2467
17. Budimir M, Jijie R, Ye R, Barras A, Melinte S, Silhanek A, Markovic Z, Szunerits S, Boukherroub R (2019) Efficient capture and photothermal ablation of planktonic bacteria and biofilms using reduced graphene oxide–polyethyleneimine flexible nanoheaters. J Mater Chem B 7:2771–2781
18. F. Halouane, R. Jijie, D. Meziane, C. Li, S. K. Singh, J. Bouckaert, J. Jurazek, S. Kurungot, A. Barras, M. Li, R. Boukherroub, S. Szunerits, Selective isolation and eradication of *E. coli* associated with urinary tract infections using anti-fimbrial modified magnetic reduced graphene oxide nanoheaters, J. Mater. Chem. B 5 (2017) 8133–8142.
19. Jiang BP, Zhang L, Zhu Y, Shen XC, Ji SC, Tan XY, Chenga L, Liang H (2015) Water-soluble hyaluronic acid–hybridized polyaniline nanoparticles for effectively targeted photothermal therapy. J Mater Chem B 3:3767–3776
20. Song XJ, Gong H, Yin SN, Cheng L, Wang C, Li ZW, Li YG, Wang XY, Liu G, Liu Z (2014) Ultra-small iron oxide doped polypyrrole nanoparticles for *in vivo* multimodal imaging guided photothermal therapy. Adv Funct Mater 24:1194–1201
21. MacNeill CM, Wailes EM, Levi-Polyachenko NH (2013) A comparative study of the photothermal efficiency of electrically conducting Poly(3,4-ethylenedioxythiophene)-based nanomaterials with cancer cells. J Nanosci Nanotechnol 13:3784–3791
22. Li Y, Jiang C, Zhang D, Wang Y, Ren X, Ai K, Chen X, Lu L (2017) Targeted polydopamine nanoparticles enable photoacoustic imaging guided chemo-photothermal synergistic therapy of tumor. Acta Biomater 47:124–134
23. Jiang BP, Zhang L, Guo XL, Shen XC, Wang Y, Zhu Y, Liang H (2017) Poly(N-phenylglycine)-based nanoparticles as highly effective and targeted near-infrared photothermal therapy/photodynamic therapeutic agents for malignant melanoma. Small 13:1602496–1602496
24. Chen H, Liang W, Zhu Y, Guo Z, Jian J, Jiang BP, Liang H, Shen XC (2018) Supercharged fluorescent protein functionalized water-soluble poly(N-phenylglycine) nanoparticles for highly effective imaging-guided photothermal therapy. Chem Commun 54:10292–10295
25. V. N. Tran, C. Dasagrandhi, V. G. Truong, Y. M. Kim, H. W. Kang, Antibacterial activity of *Staphylococcus aureus* biofilm under combined exposure of glutaraldehyde, near-infrared light, and 405-nm laser, Plos One 13(8) (2018) e0202821.
26. Gorle G, Bathinapatla A, Chen YZ, Ling YC (2018) Near infrared light activatable PEI-wrapped bismuth selenide nanocomposites for photothermal/photodynamic therapy induced bacterial inactivation and dye degradation. RSC Adv 8:19827–19834
27. A. Al-Sharqi, K. Apun, M. Vincent, D. Kanakaraju, L. M. Bilung, Enhancement of the antibacterial efficiency of silver nanoparticles against gram-positive and gram-negative bacteria using blue laser light, Int. J. Photoenergy (2019) 1–12.
28. Deng K, Li C, Huang S, Xing B, Jin D, Zeng Q, Hou Z, Lin J (2017) Recent progress in near infrared light triggered photodynamic therapy. Small 13:1702299
29. Yin M, Li Z, Ju E, Wang Z, Dong K, Ren J, Qu X (2014) Multifunctional upconverting nanoparticles for near-infrared triggered and synergistic antibacterial resistance therapy. Chem Commun 50(50):10488–10490
30. Xing C, Xu Q, Tang H, Liu L, Wang S (2009) Conjugated polymer/porphyrin complexes for efficient energy transfer and improving light-activated antibacterial activity. J Am Chem Soc 131:13117–13124
31. Wang L, He H, Zhang C, Sun L, Liu S, Wang S (2015) Antimicrobial activity of silver loaded MnO_2 nanomaterials with different crystal phases against *Escherichia coli*. J Environ Sci 41:112–120
32. Braeken Y, Cheruku S, Ethirajan A, Maes W (2017) Conjugated polymer nanoparticles for bioimaging. Materials 10(12):1420
33. Yuwen L, Sun Y, Tan G, Xiu W, Zhang Y, Weng L, Teng Z, Wang L (2018) MoS_2@polydopamine-Ag nanosheets with enhanced antibacterial activity for effective treatment of *Staphylococcus aureus* biofilms and wound infection. Nanoscale 10:16711–16720
34. Maric S, Vranes J (2017) Characteristics and significance of microbial biofilm formation. Period Biol 109(2):115–121